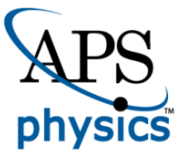

Quantum Optomechanics in a Liquid

A. B. Shkarin, A. D. Kashkanova, C. D. Brown, S. Garcia, K. Ott, J. Reichel, and J. G. E. Harris

Phys. Rev. Lett. **122**, 153601 — Published 15 April 2019

DOI: 10.1103/PhysRevLett.122.153601

Quantum optomechanics in a liquid

A. B. Shkarin,[1,*] A. D. Kashkanova,[1,*] C. D. Brown,[1]
S. Garcia,[2] K. Ott,[2] J. Reichel,[2] J. G. E. Harris[1,3,4,†]

[1] *Department of Physics, Yale University, New Haven, CT, 06520, USA*
[2] *Laboratoire Kastler Brossel, ENS-Université PSL, CNRS, Sorbonne Université, Collège de France 24 rue Lhomond, 75005 Paris, France*
[3] *Department of Applied Physics, Yale University, New Haven, CT, 06520, USA*
[4] *Yale Quantum Institute, Yale University, New Haven, CT, 06520, USA*
[*] These authors contributed equally to this work
[†] Corresponding author: jack.harris@yale.edu

We have measured the quantum fluctuations of a single acoustic mode in a volume of superfluid He that is coupled to an optical cavity. Specifically, we monitor the Stokes and anti-Stokes light scattered by a standing acoustic wave that is confined by the cavity mirrors. The intensity of these signals (and their cross-correlation) exhibit the characteristic features of the acoustic wave's zero-point motion and the quantum back action of the intracavity light. While these features have also been observed in the vibrations of solid objects and ultracold atomic gases, their observation in superfluid He opens the possibility of exploiting the remarkable properties of this material to access new regimes of quantum optomechanics.

When light interacts with a macroscopic object it typically produces complex excitations within the object that cannot be reversed by practical means. This effectively destroys the light's quantum state and precludes access to the macroscopic object's quantum dynamics. This limitation can be overcome by identifying an object with a collective degree of freedom that interacts strongly with the electromagnetic (EM) field but remains well-isolated from other degrees of freedom. Examples include superconducting circuits [1], atomic gases [2], ferromagnets [3], and objects whose vibrations couple to an EM cavity [4]. In the lattermost case (known as an optomechanical system) the object's vibrational mode is isolated by its high quality factor, while its interaction with the EM field results from radiation pressure, electrostriction, or other reversible processes [4]. Optomechanical experiments have demonstrated quantum effects in mechanical oscillators as massive as ~ 100 ng [5], as hot as ~ 300 K [6], and employing EM fields in the microwave [7,8] or near-infrared [9,10,11,12,13,5,6] domains. They have been used to realize hybrid quantum systems with superconducting qubits [7], atomic spins [13], and solid-state impurities [12], and show considerable promise in applications such as coherent microwave-to-optical conversion [14,15]. To date, the mechanical oscillators demonstrating quantum behavior have been formed from solids [5,6,7,11,12,13,9,8] or ultracold gases [10]. Here we describe measurements of quantum behavior in the vibration of a liquid body that is coupled to an optical cavity. Specifically, we monitor the dynamics of an individual acoustic standing wave in a volume of superfluid liquid helium, and observe the characteristic signatures of zero-point motion and quantum back-action [16,17,18]. This opens the possibility of exploiting the properties of liquids (and superfluid helium in particular) to access qualitatively new regimes of quantum optomechanics.

The signatures of quantum motion described here have also been measured in solid-based and gas-based optomechanical systems [5,6,9,10,11]. However their observation in a liquid is significant because of several fundamental and technical features offered by liquid-based optomechanical systems. First, liquids possess mechanical degrees of freedom (such as rotational flow) with unbounded displacement; as such they differ qualitatively from the normal modes of a solid, which represent bounded harmonic oscillations about an equilibrium [19,20]. Second, the presence of a free surface allows a liquid body's geometry and topology to be reconfigured *in situ* and to serve as a dynamical degree of freedom. Third, superfluid He can host a number of atom-like impurities (such as electrons, ions, and He_2^* excimers) potentially suitable for hybrid

quantum systems [21,22]. Fourth, the remarkable physical properties of superfluid He help to address some of the outstanding technical challenges in optomechanics: its exceptional thermal conductivity allows for effective cooling by conventional refrigerators, its acoustic damping can be predicted *a priori* [23,24], and its ability to conformally fill or coat a cryogenic EM resonator [23,24,25,26] means that such devices require no *in situ* alignment. Lastly, this type of device offers the possibility of applying precision optical measurements to address outstanding questions regarding the fundamental properties of superfluid He [27,28]. Some of the features listed above can be explored by optomechanical systems in the classical regime (using normal fluids [29,30] or superfluid He [23,24,25,26]). However the quantum regime of liquid-based optomechanics remains largely unexplored by theory and experiment.

The device used in this study is shown in Fig. 1a. It consists of a cavity formed between the end faces of two optical fibers. These end faces serve as high-reflectivity mirrors, and are mounted on the mixing chamber (MC) of a dilution refrigerator (see Supplemental Material [31]). When the cavity is excited by a laser, these mirrors confine an optical standing wave. The mode used in these experiments has frequency $\omega_{\mathrm{opt}} = 2\pi \times 196.0$ THz, linewidth $\kappa = 2\pi \times 21$ MHz, external coupling rate $\kappa_{\mathrm{ext}} = 2\pi \times 10$ MHz (including the transverse mode matching), and finesse $F = 9.5 \times 10^4$. The device is similar to the one described in Ref. [24], but offers improved thermal conductance between the cavity and the MC.

When the cavity is filled with liquid He, the fiber ends also confine acoustic modes. The acoustic modes' density variations alter the index of refraction experienced by the optical modes. Equivalently, the optical modes' intensity variations exert a force that can excite the acoustic modes. This leads [24,32] to optomechanical coupling of the conventional [4] form $H_{\mathrm{OM}} = \hbar g^{(0)} a^{\dagger} a (c^{\dagger} + c)$ where a and c are the annihilation operators for cavity photons and phonons, respectively. Straightforward geometric considerations show that the single-quantum optomechanical coupling rate $g^{(0)}$ is maximized for an acoustic mode with half the wavelength of the optical mode [24,32]. As a result, the optical mode used in this experiment couples to an acoustic mode with resonant frequency $\omega_{\mathrm{ac}} \approx 2\pi \times 319.2$ MHz.

The device was characterized using optomechanically induced transparency / amplification (OMIT/A), a standard technique in which laser tones applied to the cavity drive the acoustic mode and record its driven motion [33]. Analysis of these measurements (see

Supplemental Material [31] and Ref. [24]) provides a best-fit value of $g^{(0)} = 2\pi \times (3.6 \pm 0.1)$ kHz (unless noted, errors correspond to the statistical uncertainty in least-squared fits). This value is consistent with the *a priori* calculation (Supplemental Material [31]) $g^{(0)} = 2\pi \times (3.9 \pm 0.2)$ kHz (here the error is due to uncertainty in the mirror materials properties).[34]

In the absence of any external drive, the acoustic mode's thermal and quantum fluctuations can be inferred from the motional sidebands imprinted on a laser beam that interacts with the cavity. Standard optomechanics theory predicts that the acoustic mode's thermal fluctuations contribute equally to the red and blue motional sidebands, but that quantum fluctuations contribute unequally [4]. Specifically, when the blue sideband is converted to a photocurrent via heterodyne detection, its power spectral density $S_{ii}^{(\mathrm{bb})}$ is predicted to consist of a noise floor plus a peak that reproduces the acoustic mode's Lorentzian lineshape. When the photocurrent is appropriately calibrated (see below and the Supplemental Material [31]), the height of this peak h_{bb} equals the mode's mean phonon number n_{ac}. The same holds for $S_{ii}^{(\mathrm{rr})}$ (the photocurrent spectrum resulting from the red sideband), except that its peak height $h_{\mathrm{rr}} = n_{\mathrm{ac}} + 1$. Furthermore, the spectrum of correlations between the two sidebands ($S_{ii}^{(\mathrm{rb})}$) is predicted to have a real part consisting of the same lineshape (with height $h_{\mathrm{rb,Re}} = n_{\mathrm{ac}} + ½$) and an imaginary part with an antisymmetric lineshape of magnitude $h_{\mathrm{rb,Im}} = ½$. (Equivalent information can also be extracted by measuring both quadratures of the reflected light.[6,35])

While various interpretations can be applied to these features (see Refs. [16, 17, 18] and Supplementary Material [31]) they are intrinsically quantum in nature as the perceived energy differences between $S_{ii}^{(\mathrm{bb})}$, $S_{ii}^{(\mathrm{rr})}$, and $S_{ii}^{(\mathrm{rb})}$ are set by the energy of a single phonon $\hbar\omega_{\mathrm{ac}}$. It is convenient to characterize these quantum features by three parameters: $H_{\mathrm{AS}} \equiv h_{\mathrm{rr}} - h_{\mathrm{bb}}$, $H_{\mathrm{Re}} \equiv 2(h_{\mathrm{rb,Re}} - h_{\mathrm{bb}})$, and $H_{\mathrm{Im}} \equiv 2h_{\mathrm{rb,Im}}$. Each is predicted to be unity, independent of experimental conditions such as temperature and laser power.

The system described here operates well in the resolved sideband regime ($\omega_{\mathrm{ac}} \approx 15\,\kappa$), so it is impractical to measure the two sidebands produced from a single beam (at least one will be strongly suppressed by the cavity's response). Instead, we apply two measurement beams to the cavity: an "upper" beam with detuning (relative to the cavity resonance) $\Delta_{\mathrm{u}} = \omega_{\mathrm{ac}} + \delta$ and a "lower" beam with detuning $\Delta_{\ell} = -\omega_{\mathrm{ac}} - \delta$ where δ is set to $2\pi \times 100$ kHz. As illustrated in the inset of Fig. 2 this ensures that two motional sidebands are approximately resonant with the

cavity: the lower beam's blue sideband, and the upper beam's red sideband. The offset δ is chosen so that these sidebands do not overlap, but do lie within the measurement bandwidth. The sidebands are recorded simultaneously via a heterodyne measurement and $S_{ii}^{(\mathrm{bb})}$, $S_{ii}^{(\mathrm{rr})}$, and $S_{ii}^{(\mathrm{rb})}$ are computed from this record (Supplemental Material [31]). Each of these records is calibrated (Supplemental Material [31]) so that the features in $S_{ii}^{(\mathrm{bb})}$, $S_{ii}^{(\mathrm{rr})}$, and $S_{ii}^{(\mathrm{rb})}$ should be related to n_{ac} as described above.

Figure 2 shows a typical measurement of $S_{ii}^{(\mathrm{rr})}$ and $S_{ii}^{(\mathrm{bb})}$ (with their frequency-independent background subtracted) as well as $S_{ii}^{(\mathrm{rb})}$. The features in this data appear qualitatively consistent with the quantum effects described above. To quantify this comparison we fit $S_{ii}^{(\mathrm{rr})}$, $S_{ii}^{(\mathrm{bb})}$, and $\mathrm{Re}(S_{ii}^{(\mathrm{rb})})$ to the function $h_x / (1+4(\omega-\omega_{\mathrm{ac}})^2/\gamma_{\mathrm{ac}}^2)$ with x = {rr; bb; rb,Re}, while $\mathrm{Im}(S_{ii}^{(\mathrm{rb})})$ is fit to $h_{\mathrm{rb,Im}}(\omega-\omega_{\mathrm{ac}})(\gamma_{\mathrm{ac}}/2)^{-1}(1+4(\omega-\omega_{\mathrm{ac}})^2/\gamma_{\mathrm{ac}}^2)^{-1}$ (Supplemental Material [31]). Here ω is the measurement frequency, and ω_{ac} and γ_{ac} are the acoustic mode's frequency and linewidth. The fits in Fig. 2 give $H_{\mathrm{AS}} = 1.10 \pm 0.086$, $H_{\mathrm{Re}} = 0.97 \pm 0.14$, $H_{\mathrm{Im}} = 1.06 \pm 0.055$.

The parameters H_{AS}, H_{Re}, and H_{Im} are defined to reflect only the quantum aspects of the system's dynamics; however they are determined from fit parameters (h_{bb}, h_{rr}, $h_{\mathrm{rb,Re}}$, and $h_{\mathrm{rb,Im}}$) that reflect both thermal and quantum fluctuations. To compare the quantum and thermal signatures in the data, we measured heterodyne spectra similar to those in Fig. 2 over a range of T_{MC} (the MC temperature) and n_{circ} (the intracavity photon number). Figure 3a,b shows the inferred phonon number of the acoustic mode's bath, defined as $n_{\mathrm{th}} = n_{\mathrm{ac}}(\gamma_{\mathrm{ac}}/\gamma_{\mathrm{ac},0}) - n_{\mathrm{O}}\gamma_{\mathrm{O}}/\gamma_{\mathrm{ac},0}$. This expression was evaluated by fitting heterodyne spectra (as in Fig. 2) for γ_{ac} and n_{ac} (for these measurements we use $n_{\mathrm{ac}} = \frac{1}{2}(h_{\mathrm{bb}} + h_{\mathrm{rr}} - 1)$). Standard optomechanics theory [4] was used to calculate the phonon number associated with the quantum back-action n_{O} and the optical damping rate $\gamma_{\mathrm{O}} = \gamma_{\mathrm{ac}} - \gamma_{\mathrm{ac},0}$ (where $\gamma_{\mathrm{ac},0}$ is the acoustic damping rate when $n_{\mathrm{circ}} = 0$). For all the measurements described here n_{th} nearly equals n_{ac}, as the "quantum back-action" term $n_{\mathrm{O}}\gamma_{\mathrm{O}}/\gamma_{\mathrm{ac}} < 1.1$, and the "laser cooling" factor $\gamma_{\mathrm{ac}}/\gamma_{\mathrm{ac},0}$ differs from unity by no more than 5%.[36] We plot n_{th} (rather than n_{ac}) in Fig. 3a,b to facilitate comparison with the thermal model described in the Supplemental Material [31].

Figure 3a shows n_{th} versus T_{MC}. For $T_{\mathrm{MC}} \gtrsim 150$ mK n_{th} tracks T_{MC}, while for $T_{\mathrm{MC}} \lesssim 150$ mK n_{th} does not track T_{MC} and clearly depends on n_{circ}. Qualitatively similar behavior was found in Ref. [24], and was accounted for by a thermal model in which the He temperature was set by

the heat from optical absorption in the mirrors and the cooling provided by the slender superfluid region which linked that device to the MC. The present device's more open geometry gives improved cooling, but the absence of a thermal bottleneck means that the temperature is not uniform throughout the cavity. We calculate the cavity's temperature distribution using standard models of thermal transport and convert this distribution into an effective temperature for the mode T_{eff} that depends upon T_{MC} and n_{circ} (Supplemental Material [31]). Fig. 3b shows the same values of n_{th} as Fig. 3a, but plotted versus T_{eff}. In this case the data shows close agreement with the prediction $n_{\mathrm{th}} = 1/(e^{\hbar\omega_{\mathrm{ac}}/k_{\mathrm{B}}T} - 1)$ over the full range of T_{MC} and n_{circ}, indicating that this approach captures the main features of the device's thermal behavior. The deviations from the prediction are roughly independent of T_{MC} and n_{circ}, and so are unlikely to arise from thermal effects (which would typically depend on T_{MC} and n_{circ}). Instead, this behavior is consistent with an imperfect calibration of the heterodyne signal (Supplemental Material [31]).

Figure 3c shows H_{AS}, H_{Re}, and H_{Im} as a function of T_{eff}. The points in Fig. 3c are derived from data and fits similar to those in Fig. 2 (and from the same set of measurements used to produce Fig. 3a, b). The uncertainty grows at higher T_{eff} because of the rapid increase of γ_{ac} with T_{eff}, which makes the motional sidebands harder to distinguish from the noise floor. The uncertainty also grows at the lowest values of T_{eff} owing to the need to use low n_{circ}. The data in Fig. 3c are consistent with the theoretical prediction (dashed line), indicating their origin in the coherent quantum dynamics of the cavity's acoustic and optical modes.

In conclusion, we have isolated a single normal mode of a liquid body and measured its quantum fluctuations. This result is distinct from the large body of work on the quantum aspects of superfluid He's bulk properties, which reflect the aggregate behavior of very many normal modes. It is also distinct from work on quantum effects directly related to the superfluid's wavefunction (such as persistent flow, quantized vortices, and Josephson effects); although superfluidity greatly facilitates the experiments described here by suppressing the viscous damping of the acoustic mode, the acoustic mode itself and its quantum dynamics are generic to any liquid.

We thank Vincent Bernardo, Kjetil Børkje, Glen Harris, and Hong Tang for their assistance, and LaserOptik GmbH for depositing the mirror coatings. We acknowledge financial support from W. M. Keck Foundation Grant No. DT121914, AFOSR Grant FA9550-15-1-0270,

DARPA Grant W911NF-14-1-0354, ONR MURI on Quantum Optomechanics (Award No. N00014-15-1-2761), ARO Grant W911NF-13-1-0104, and NSF Grant 1205861. This work has been supported by the DARPA/MTO ORCHID program through a grant from AFOSR. This project was made possible through the support of a grant from the John Templeton Foundation. The opinions expressed in this publication are those of the authors and do not necessarily reflect the views of the John Templeton Foundation. This material is based upon work supported by the National Science Foundation Graduate Research Fellowship under Grant No. DGE-1122492. S.G., K.O. and J.R. acknowledge funding from the EU Information and Communication Technologies program (QIBEC project, GA 284584), ERC (EQUEMI project, GA 671133), and IFRAF.

References

[1] M. H. Devoret and R. J. Schoelkopf, *Science* **339**, 1169 (2013).

[2] D. M. Stamper-Kurn in *Cavity Optomechanics*, edited by M. Aspelmeyer, T. J. Kippenberg and F. Marquardt (Springer, Heidelberg-New York-Dordrecht-London, 2014) pp. 283-325.

[3] T. Tabuchi, S. Ishino, A. Noguchi, T. Ishikawa, R. Yamazaki, K. Usami, and Y. Nakamura, *Science* **349**, 405 (2015).

[4] M. Aspelmeyer, T. J. Kippenberg and F. Marquardt, *Rev. Mod. Phys.* **86**, 1391 (2014).

[5] M. Underwood, D. Mason, D. Lee, H. Xu, L. Jiang, A. B. Shkarin, K. Børkje, S. M. Girvin, and J. G. E. Harris, *Phys. Rev. A* **92**, 061801(R) (2015).

[6] T. P. Purdy, K. E. Grutter, K. Srinivasan and J. M. Taylor, *Science* **356**, 1265 (2017).

[7] A. D. O'Connell, M. Hofheinz, M. Ansmann, R. C. Bialczak, M. Lenander, E. Lucero, M. Neeley, D. Sank, H. Wang, M. Weides, J. Wenner, J. Martinis and A. N. Cleland, *Nature* **464**, 697 (2010).

[8] T. A. Palomaki, J. D. Teufel, R. W. Simmonds and K. W. Lehnert, *Science* **342**, 710-713 (2013).

[9] A. H. Safavi-Naeini, J. Chan, J. T. Hill, T. P. Mayer Alegre, A. Krause and O. Painter, *Phys. Rev. Lett.* **108**, 033602 (2012).

[10] N. Brahms, T. Botter, S. Schreppler, D. W. C. Brooks and D. M. Stamper-Kurn, *Phys. Rev. Lett.* **108**, 133601 (2012).

[11] T. P. Purdy, P. L. Yu, N. S. Kampel, R. W. Peterson, K. Cicak, R. W. Simmonds and C. Regal, *Phys. Rev. A* **92**, 031802(R) (2015).

[12] D. A. Golter, T. Oo, M. Amezcua, K. A. Stewart and H. Wang, *Phys. Rev. Lett.* **116**, 143602 (2016).

[13] C. B. Møller, R. A. Thomas, G. Vasilakis, E. Zeuthen, Y. Tsaturyan, K. Jensen, A. Schliesser, K. Hammerer and E. S. Polzik, *Nature* **547**, 191 (2017).

[14] J. Bochmann, A. Vainsencher, D. D. Awschalom and A. N. Cleland, *Nat. Phys.* **9**, 712 (2013).

[15] R. W. Andrews, R. W. Peterson, T. P. Purdy, K. Cicak, R. W. Simmonds, C. A. Regal and K. W. Lehnert, *Nat. Phys.* **10**, 321 (2014).

[16] F. Ya. Khalili, H. Miao, H. Yang, A. H. Safavi-Naeini, O. Painter and Y. Chen, *Phys. Rev. A* **86**, 033840 (2012).

[17] A. J. Weinstein, C. U. Lei, E. E. Wollman, J. Suh, A. Metelmann, A. A. Clerk and K. C. Schwab, *Phys. Rev. X* **4**, 041003 (2014).

[18] K. Børkje, *Phys. Rev. A* **94**, 043816 (2016).

[19] M. Bhattacharya, *J. Opt. Soc. Am. B* **32,** B55 (2017).

[20] L. Childress, M. P. Schmidt, A. D. Kashkanova, C. D. Brown, G. I. Harris, A. Aiello, F. Marquardt and J. G. E. Harris, *Phys. Rev. A* **96,** 063842 (2017).

[21] S. A. Lyon, Phys. Rev. A **74**, 052338 (2006).

[22] P. M. Platzman and M. I. Dykman, *Science* **284**, 1967-1969 (1999).

[23] L. A. De Lorenzo and K. C. Schwab, *New J. Phys.* **16**, 113020 (2014).

[24] A. D. Kashkanova, A. B. Shkarin, C. D. Brown, N. E. Flowers-Jacobs, L. Childress, S. W. Hoch, L. Hohmann, K. Ott, J. Reichel and J. G. E. Harris, *Nat. Phys.* **13**, 74 (2017).

[25] G. I. Harris, D. L. McAuslan, E. Sheridan, Y. Sachkou, C. Baker and W. P. Bowen, *Nat. Phys.* **12**, 788 (2016).

[26] F. Souris, X. Rojas, P. H. Kim and J. P. Davis, *Phys. Rev. Appl.* **7**, 044008 (2017).

[27] W. F. Vinen, M. Tsubota and A. Mitani, *Phys. Rev. Lett.* **91**, 135301 (2003).

[28] E. Kozik and B. Svistunov, *Phys. Rev. Lett.* **92**, 035301 (2004).

[29] G. Bahl, K. H. Kim, W. Lee, J. Liu, X. Fan and T. Carmon, *Nat. Comm*. **4**, 1994 (2013).

[30] S. Kaminski, L. L. Martin, S. Maayani and T. Carmon, *Nat. Phot.* **10**, 758 (2016).

[31] See Supplemental Material for details of the experimental apparatus, characterization measurements, calibration procedures, and theoretical modelling of the optical signals and thermal behavior, which includes Refs. [37-57].

[32] G. S. Agarwal and S. S. Jha, *Phys. Rev. A* **90**, 023812 (2014).

[33] S. Weis, R. Rivière, S. Deléglise, E. Gavartin, O. Arcizet, A. Schliesser and T. J. Kippenberg, *Science* **330**, 1520 (2010).

[34] These measurements also provide a measure of the non-unitary phothermal effects in the system. As described in Section 3.4 of Ref. [31], they do not contribute appreciably to the measurements presented here.

[35] K. Børkje, A. Nunnenkamp, B. M. Zwickl, C. Yang, J. G. E. Harris and S. M. Girvin, *Phys. Rev. A* **82**, 013818 (2010).

[36] The near absence of laser cooling in these measurements results because the two measurement tones are detuned symmetrically (relative to the cavity resonance) to within ~ 0.01 κ, leading to cancellation of their dynamical back action. See Ref. [33] Section 2.3 for details.

Figure Captions

Figure 1 | Schematic of the experiment. a, Top: Illustration of the optomechanical device. The optical fibers (yellow) and ferrules (white) are fixed inside a Cu cell (gray) which is attached to the mixing chamber of a dilution refrigerator (DR, not shown). Liquid He (blue) fills the cell. The fibers enter the cell via epoxy feedthroughs (black). Bottom: enlarged view of the cavity. Red curve: the intensity profile of an optical mode; blue shading: the density profile of the acoustic mode that couples to the optical mode. The actual optical and acoustic modes used in this work have, respectively, 91 and 182 half-wavelengths along the cavity length. **b**, Simplified layout of the measurement setup. Light from a tunable laser (TL) passes through a phase modulation system (□M) driven by a microwave source (MW). Light is delivered to (and collected from) the DR via a circulator (pink). The reflected light is collected on a photodiode (PD), and the resulting photocurrent is analyzed by a data acquisition system (DAQ). Details are given in Supplemental Material [31].

Figure 2 | Sidebands produced by the acoustic mode's fluctuations. Inset: Illustration of the measurement scheme. Black curve: cavity lineshape. Colored arrows: laser tones. Colored curves: acoustic sidebands. Upper panel: the spectrum of the red and blue motional sidebands ($S_{ii}^{(\mathrm{rr})}$ and $S_{ii}^{(\mathrm{bb})}$) and the real part of their cross-correlation ($\mathrm{Re}[S_{ii}^{(\mathrm{rb})}]$). A frequency-independent background has been subtracted from $S_{ii}^{(\mathrm{rr})}$ and $S_{ii}^{(\mathrm{bb})}$. Lower panel: the imaginary part of the cross-correlation ($\mathrm{Im}[S_{ii}^{(\mathrm{rb})}]$). The data were normalized and fit as described in the text and the Supplemental Material [31]. For this measurement T_{MC} = 20 mK and n_{circ} = 400.

Figure 3 | Thermal and quantum fluctuations of the acoustic mode. a, The mean phonon number n_{th} associated with the acoustic mode's bath temperature, plotted versus T_{MC}. **b**, The same measurements of n_{th} as in **a** but plotted as a function of T_{eff}, the effective device temperature calculated in the Supplemental Material [31]. The color of each marker encodes n_{circ},

the intracavity photon number. The black points are obtained by averaging data in 15 mK bins. In both **a** and **b** the dashed lines show the expected behavior $n_{\mathrm{th}} = 1/(e^{\hbar\omega_{\mathrm{ac}}/k_{\mathrm{B}}T} - 1)$, while the grey area represents the systematic uncertainty resulting from the calibration of the heterodyne signal (Supplemental Material [31]). **c**, Three measures of the quantum features, plotted as a function of T_{eff}. The dashed line is the prediction of quantum optomechanics theory; the grey area shows the systematic uncertainty resulting from the calibration of the heterodyne signal. Each data point is produced from data and fits similar to Fig. 2 (averaged over 15 mK bins). Error bars indicate the statistical uncertainty in these fits.

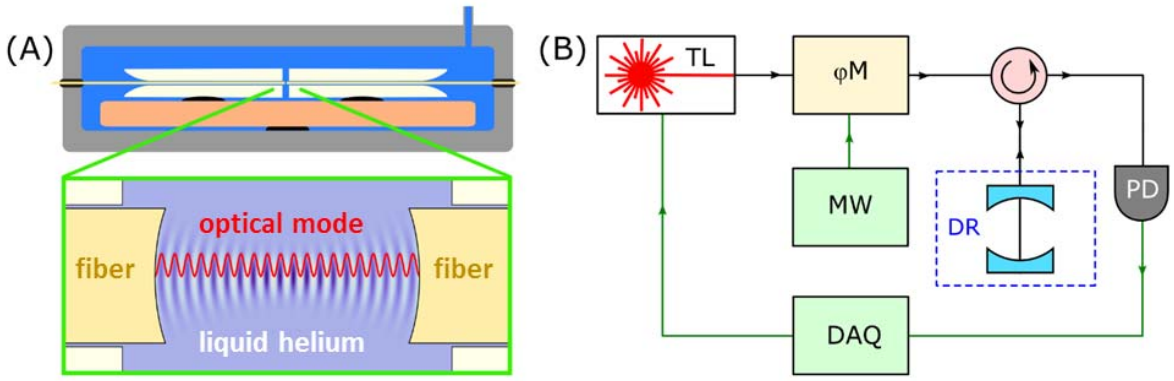

Figure 1

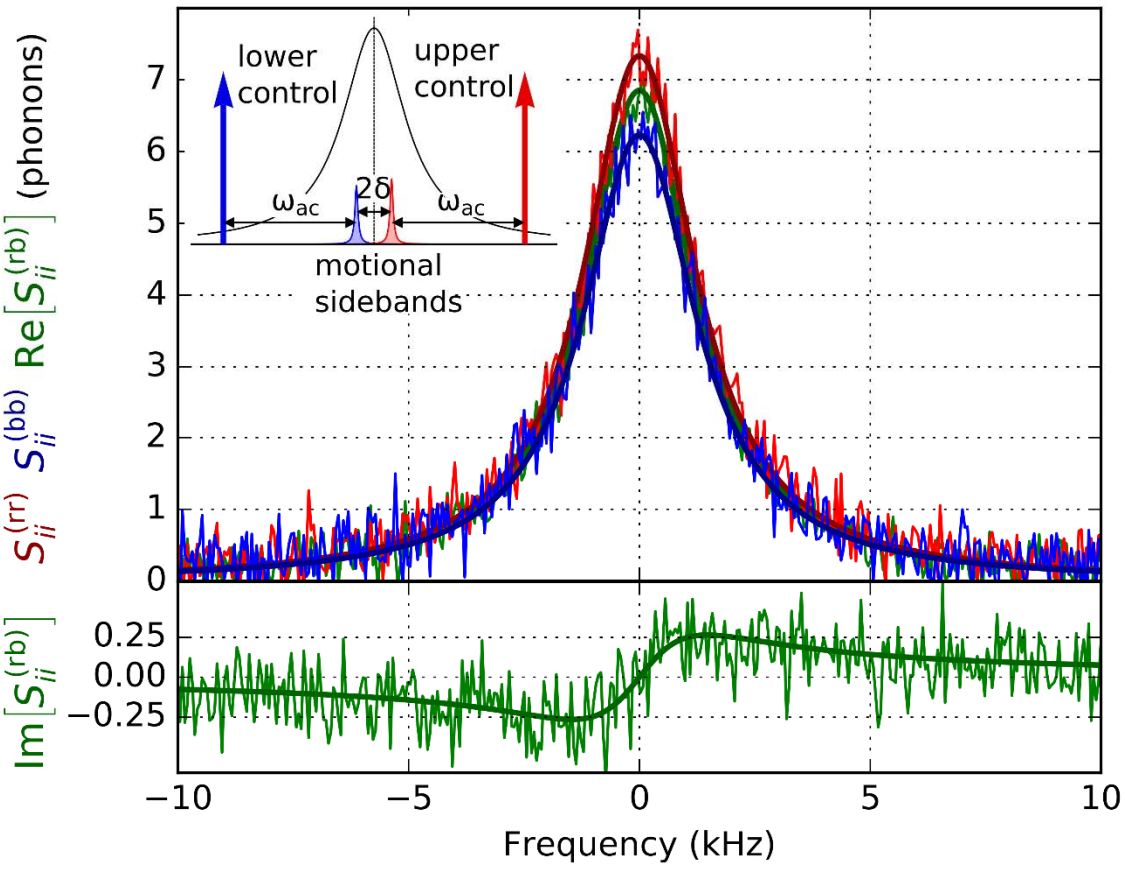
lower
control
upper
control
2δ
ω_ac
ω_ac
motional
sidebands
$S_{ii}^{(rr)}$ $S_{ii}^{(bb)}$ $\mathrm{Re}\left[S_{ii}^{(rb)}\right]$ (phonons)
$\mathrm{Im}\left[S_{ii}^{(rb)}\right]$
Frequency (kHz)

Figure 2

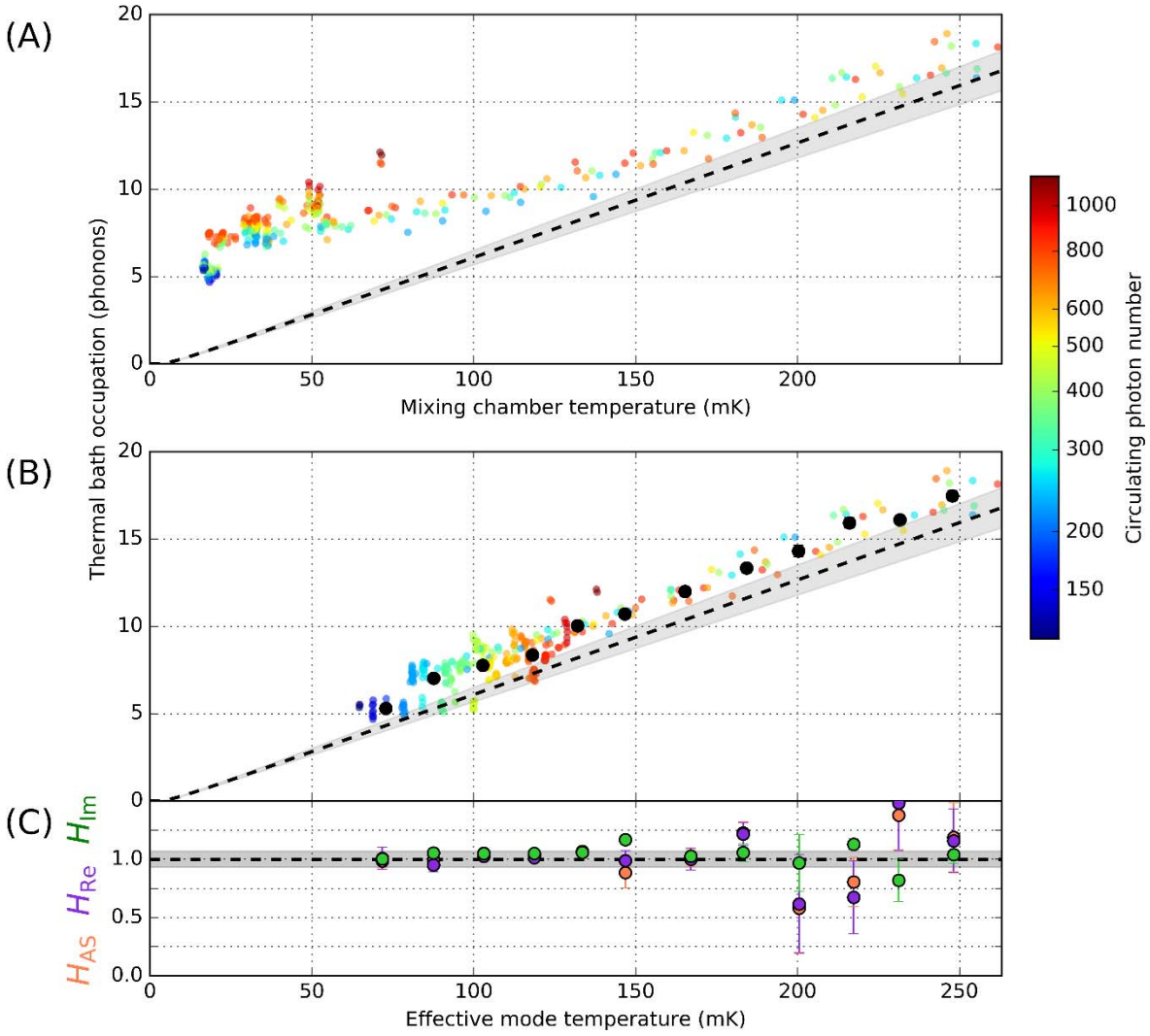
(A)
(B)
(C)
Thermal bath occupation (phonons)
Mixing chamber temperature (mK)
Effective mode temperature (mK)
Circulating photon number
1000
800
600
500
400
300
200
150
H_{AS}
H_{Re}
H_{Im}

Figure 3